Anvil glaciation in a deep cumulus updraught over Florida simulated with the Explicit Microphysics Model. I: Impact of various nucleation processes

By VAUGHAN T. J. PHILLIPS[1]†, CONSTANTIN ANDRONACHE[2], STEVEN C. SHERWOOD[3], AARON BANSEMER[4], WILLIAM C. CONANT[5], PAUL J. DEMOTT[6], RICHARD C. FLAGAN[5], ANDY HEYMSFIELD[4], HAFLIDI JONSSON[7], MICHEAL POELLOT[8], TRACEY A. RISSMAN[5], JOHN H. SEINFELD[5], TIM VANREKEN[5], VARUNTIDA VARUTBANGKUL[5] and JAMES C. WILSON[9]

[1]*Atmospheric and Oceanic Sciences Program, Princeton University, New Jersey, USA*
[2]*Boston College, Chestnut Hill, Massachusetts, USA*
[3]*Department of Geology, Yale University, New Haven, USA*
[4]*National Centre for Atmospheric Research, Boulder, Colorado, USA*
[5]*Department of Environmental Science and Engineering, Caltech, Pasadena, California, USA*
[6]*Department of Atmospheric Science, Colorado State University, Fort Collins, Colorado, USA*
[7]*Center for Interdisciplinary Remotely-Piloted Aircraft Studies, Monterey, California, USA*
[8]*Department of Atmospheric Sciences, University of North Dakota, USA*
[9]*University of Denver, Colorado, USA*

SUMMARY

Simulations of a cumulonimbus cloud observed in the Cirrus Regional Study of Tropical Anvils and Cirrus Layers–Florida Area Cirrus Experiment (CRYSTAL-FACE) with an advanced version of the Explicit Microphysics Model (EMM) are presented. The EMM has size-resolved aerosols and predicts the time evolution of sizes, bulk densities and axial ratios of ice particles. Observations by multiple aircraft in the troposphere provide inputs to the model, including observations of the ice nuclei and of the entire size distribution of condensation nuclei.

Homogeneous droplet freezing is found to be the source of almost all of the ice crystals in the anvil updraught of this particular model cloud. Most of the simulated droplets that freeze to form anvil crystals appear to be nucleated by activation of aerosols far above cloud base in the interior of the cloud ('secondary' or 'in-cloud' droplet nucleation). This is partly because primary droplets formed at cloud base are invariably depleted by accretion before they can reach the anvil base in the updraught, which promotes an increase with height of the average supersaturation in the updraught aloft. More than half of these aerosols, activated far above cloud base, are entrained into the updraught of this model cloud from the lateral environment above about 5 km above mean sea level. This confirms the importance of remote sources of atmospheric aerosol for anvil glaciation.

Other nucleation processes impinge indirectly upon the anvil glaciation by modifying the concentration of supercooled droplets in the upper levels of the mixed-phase region. For instance, the warm-rain process produces a massive indirect impact on the anvil crystal concentration, because it determines the mass of precipitation forming in the updraught. It competes with homogeneous freezing as a sink for cloud droplets. The effects from turbulent enhancement of the warm-rain process and from other nucleation processes on the anvil ice properties are assessed.

KEYWORDS: Aerosol particles   Homogeneous aerosol freezing   Secondary droplet nucleation

1. INTRODUCTION

Cirrus cloud forms at temperatures colder than about $-30\,°C$. It covers about 35% of the globe and is fundamental to the radiation budget of the climate system (Ramanathan *et al.* 1983). Much tropical cirrus originates from the anvils of cumulonimbus (Cb) storms. An anvil is formed by the upwelling of condensate in the updraught of the storm. The rate of generation of crystals in Cb updraughts may affect the eventual ice concentration in this cirrus.

Cloud droplets are nucleated by activation of cloud condensation nuclei (CCN) aerosols either at cloud base ('primary droplet nucleation') or later in the interior of

---

the cloud ('secondary droplet nucleation'). Spontaneous ('homogeneous') freezing of activated drops occurs at temperatures colder than a size-dependent threshold, which is usually somewhere near $-36\,°C$. Supercooled cloud-droplets and raindrops may also freeze by the activation of ice nuclei (IN; 'heterogeneous ice nucleation') at subzero temperatures. In the anvil, aerosols can persist unactivated in the supercooled state until they freeze spontaneously ('homogeneous aerosol freezing') at high supersaturations with respect to ice approaching 50% or more (Jensen *et al.* 1998; Koop *et al.* 2000).

Ovtchinnikov *et al.* (2000) found that the mixed-phase microphysics of a moderate cumulus cloud with no anvil was dominated by the Hallett–Mossop (H-M) process (Hallett and Mossop 1974) of ice particle multiplication. The H-M process involves the production of splinters during the riming of large cloud droplets of >24 microns diameter onto ice at -3 to $-8\,°C$. Such mixed-phase microphysical processes, as well as warm processes, might be expected to modify the updraught's supply of condensate, aerosols and vapour to the anvil.

Turbulence in clouds has impacts on the formation of cloud droplets, on condensation growth, and on subsequent collisions and coalescence of droplets (Jonas 1996; Smith and Jonas 1996; Khain *et al.* 2000). The evolution of the cloud-droplet distribution is influenced by turbulence due to: (i) fluctuations in the supersaturation field, affecting condensation; and (ii) increased average rates of collisions, arising from fluctuations both in the droplet concentration and the relative velocity between droplets of different sizes. Turbulence affects the cloud dynamics by mixing air from the environment into the cloud. Such entrainment reduces the cloud buoyancy and dilutes condensate.

The general importance of homogeneous freezing in ice clouds is evident from the fact that liquid water is only very rarely observed at temperatures colder than about $-38\,°C$ (DeMott *et al.* 1997). Heymsfield and Sabin (1989) highlighted the potential for competition between heterogeneous and homogeneous nucleation of crystals in cirrus (see also DeMott *et al.* 1997; Spice *et al.* 1999), with homogeneous freezing favoured at stronger updraught speeds. The predominance of homogeneous freezing in observed wave-clouds with updraught speeds exceeding $1\,m\,s^{-1}$ was inferred by Heymsfield and Miloshevich (1993, 1995). Updraughts extending into Cb anvils are much faster than this, which might seem to implicate homogeneous freezing as their key mechanism for glaciation. In observational studies of Cb anvils, two types of homogeneous freezing have been proposed: first, Knollenberg *et al.* (1993) speculated that homogeneous aerosol freezing might explain high concentrations, $>10\,cm^{-3}$, of crystals observed in tropical Cb clouds; second, Rosenfeld and Woodley (2000) invoked massive homogeneous freezing of activated cloud-droplets to explain aircraft observations of some Texan convective storms.

In this paper we describe explicit microphysical calculations to evaluate the relative importance of these various mechanisms for the formation of anvil ice particles in a deep convective updraught. We also assess the modulation of such mechanisms by the warm- and mixed-phase microphysical processes. Relevant turbulence parameters are prescribed from aircraft observations and three-dimensional (3-D) model results. An advanced version of the Explicit Microphysics Model (EMM) developed by Phillips (2001) and Phillips *et al.* (2001, 2002, 2003) is applied to simulate a Cb case observed in the Cirrus Regional Study of Tropical Anvils and cirrus Layers—Florida Area Cirrus Experiment (CRYSTAL-FACE, Jensen *et al.* 2004). This is the first project, to our knowledge, to combine simultaneous measurements of aerosol particles in the lower and upper troposphere with *in situ* aircraft observations of Cb clouds and their anvil cirrus.

2. THE MODEL

(a) Overview

The EMM was originally developed by Phillips (2001) as an extension to the 1-D Multi-Thermal Model (MTM) of cumulus glaciation by Blyth and Latham (1997). Fully interactive components for vapour, cloud water, ice and rain were added to the model by Phillips. Precipitation 'size-bins' are advected in 2-D in the vertical plane on which the updraught and downdraught are located (see subsection 2(b) for a description of dynamical regions), while cloud-water size-bins and vapour are advected in 1-D. The cloud dynamics are prescribed.

Ice particles are grouped into several basic species in the model, according to their mode of formation:

(i)   Homogeneously frozen cloud droplets and aerosol particles;
(ii)   Primary ice, nucleated by condensation/deposition freezing (Meyers *et al.* 1992) between -5 and $-30\,^{\circ}$C (see subsection 3(a));
(iii) Homogeneously frozen precipitation particles;
(iv)   H-M splinters emitted from particles in species (ii) and (iii);
(v)   Frozen raindrops formed heterogeneously and from collisions with ice in species (ii)–(iv); and finally,
(vi)   Further generations of H-M splinters and raindrops frozen in collisions with H-M splinters.

For primary nucleation of crystals, contact nucleation is omitted since thermophoretic effects tend effectively to inhibit it in the convective updraught (Phillips *et al.* 2001, 2002; see also Ovtchinnikov *et al.* 2000). The observed dependence of the H-M process (Hallett and Mossop 1974) on the riming rate, temperature and droplet size are all represented: one splinter is generated for every 200 droplets $>24\,\mu$m diameter that are rimed at $-5\,^{\circ}$C. This multiplication rate is applied for all sizes of riming ice particle (see Saunders and Hosseini 2000). Homogeneous freezing of droplets of a given size occurs when the temperature falls below their size-dependent threshold (see Pruppacher and Klett 1997). The approximation is made that this freezing occurs instantaneously; the justification for this is that the time-scale for homogeneous freezing of a single cloud-droplet ($\sim 10\,\mu$m) is probably a few seconds (assuming a volumetric nucleation rate of $10^8\,$cm^{-3}s^{-1} and a cooling rate of about 10 degC minute^{-1}), which is substantially less than the time taken (about 20 s) for model updraught parcels to ascend through the layer in which 99% of their cloud-water mass is homogeneously frozen. For each basic species, the evolution of its size distribution with time is predicted in all layers in the cloud.

In the EMM, a particle-growth scheme predicts the continuous evolution of the dimensions, bulk density and axial ratio of ice particles in each size-bin (see Phillips *et al.* 2001, 2002, 2003). 'Categorization assumptions' that prescribe the shape and bulk density of ice particles in artificial classes are not in general utilized by the EMM, in contrast with many cloud models. The *continuum* of values of shape and bulk density across the size distribution that is typically seen in a given volume of cloud in nature, is represented in the EMM. Every size-bin has a 'memory' of the prior history of growth of its particles; particle properties are not simply diagnosed from the current size or mass of the particle. Ice particles are represented as either cylindrical or spheroidal shapes depending on their amount of accreted rime, and have a continuously evolving axial ratio. In contrast with many microphysical models, the EMM utilizes a variable size grid

for hydrometeors: the size of each size-bin varies continuously with time, following the motion and growth of its particles.

(b) Prescribed cloud dynamics

A 1-D dynamical framework for the cloud is prescribed in the manner described by Phillips *et al.* (2001, 2002, 2003). Values of dynamical parameters are adjusted to match observed values from the CRYSTAL-FACE Cb case of 18 July 2002, simulated here. There is a sequence of thermals in the updraught ascending at about half the local value of the peak updraught speed (see Levine 1959), which increases linearly with height between the cloud base and 11 km above mean sea level (AMSL). These thermals lift the cloud top in stages to its maximum altitude, as in the original MTM. A downdraught 1 km deep is included adjacent to each thermal. Particles are swept into the downdraught from the tops of the thermals. Ice particles in the downdraught are evaporated at a rate that is such as to maintain exact ice saturation. A model component to represent the surrounding cloudy region (SCR), introduced by Phillips *et al.* (2003) in stratiform simulations, is retained in the current version. Particles surviving descent in the downdraught are partially recirculated back into the updraught, with the remainder being deposited in the SCR. These 1-D channels, for the updraught and SCR, are discretized as stacks of ascending horizontal layers that are each about 50 m deep. The microphysical interactions are evaluated separately in each layer, and particles may fall from one layer to the next. The slope of the channels is determined by the horizontal advection of thermals by the environmental vertical shear.

The entraining mass flux of environmental air entering the updraught per unit of altitude (z), E_z (kg s^{-1}m^{-1}), is related to the updraught mass flux, $F(z)$, by: $E_z = f_E^*(z)E\Phi$, with $\Phi = F(z)/H(t)$. Here $H(t)$ is the instantaneous depth of the cloud at time t. The skew factor is defined by $f_E^*(z) = f_E(z)(H(t) - z)/H(t)$. In this case $f_E(z)$ is unity except in the upper third of each thermal where it is 0.5, and in the central third of the thermal where it is interpolated from 0.5 to unity. This parametrizes the adiabatic cores seen in aircraft observations by Heymsfield *et al.* (1978). Finally, E is an entrainment parameter that is adjusted to obtain a match of the passive tracer profile between the EMM and a 3-D model at all levels (see subsection 3(b)). Details of previous versions of the EMM are provided by Phillips *et al.* (2001, 2002, 2003).

(c) New features of model

There are some novel features of the EMM used here. First, there is now a solution of the stochastic collection equation (SCE) for coalescence, aggregation and rain–ice collisions. This replaces the autoconversion formulae in previous model versions. The scheme proposed by Bott (1998) has been adapted for the variable size grid of the EMM. In the case of aggregation, solution of the SCE involves transferral of ice crystal properties (bulk density, shape, meltwater mass, trajectory position) between size-bins whenever ice mass is transferred. For aggregation, the bulk density of aggregates at the instant of their formation is derived from empirical relations for unrimed snow crystals, and their initial axial ratio is assigned an empirical value of 0.25 (see Pruppacher and Klett 1997). Of course, during subsequent growth, the bulk density and shape of aggregates are free to evolve as predicted by the particle-growth scheme (see subsection 2(a)). Sticking efficiencies of Mitchell (1988) are applied, as in previous model versions.

The turbulent enhancement of the collision kernel occurs by the turbulent/inertia mechanism proposed and implemented by Khain and Pinsky (1995), Pinsky and Khain

(1998, 2002), Pinsky *et al.* (2000) and Khain *et al.* (2004). By this mechanism, there is a modification of the relative velocities of drops of different masses owing to their inertia. Values of the turbulent enhancement factor for coalescence are identical to those applied in the Hebrew University Cloud Model (HUCM, Khain *et al.* 2004). This enhancement factor in a given collision is a 2-D function of the masses of collecting and collector droplets. The turbulent dissipation rate assumed for their derivation is similar to the value observed by aircraft in the deep-cumulus case being simulated for this paper (see subsection 3(a)). Similarly, for riming, a 2-D set of mass-dependent turbulent enhancement factors is applied, again using HUCM data. The same set of turbulent enhancement factors is applied for 'collisional' raindrop-freezing, as for riming. Values of the (non-turbulent) drop–drop collision efficiency are those utilized by Khain and Sednev (1996) and Khain *et al.* (2004), being based on data derived theoretically and numerically by Hall (1980). Raindrop break-up is also included with Bleck's (1970) numerical method.

Explicit representation of the entire size distribution of unactivated condensation nuclei (CN) aerosols in 33 fixed doubling bins, on a grid of the dry mass of the solute, has been introduced (giant and ultra-giant aerosols are neglected—see section 6). This enhances the representation of droplet nucleation. For the jth size-bin of unactivated CN, the rate of change of the particle-number mixing ratio (number of particles per kg of air) is given by an equation similar to that for vapour and cloud water:

$$\mathrm{D}N_j/\mathrm{D}t = \alpha_{\mathrm{E}}(N_{\mathrm{env}, j}(z) - N_j) + S_j.$$

Here, α_{E} is the fractional entrainment coefficient for the updraught and is determined by E_z. Also, $N_{\mathrm{env}, j}(z)$ is the observed number mixing ratio of CN in the environment in the jth size-bin (see subsection 3(a)), while S_j is a source/sink term that accounts for losses of aerosol due to droplet nucleation. A droplet-nucleation scheme similar to that applied by Khain *et al.* (2004) has been included. For a given supersaturation, the critical CN radius is computed using Kohler theory (see Rogers and Yau 1991) assuming that the aerosols all have the same chemical composition. CN with radii exceeding this critical value are activated as cloud droplets. For an assumed chemical composition of ammonium sulphate (see subsection 3(a)), a Van't Hoff factor of three, an average molecular weight of 132.14 and a dry density of 1.77 g cm^{-3} are utilized.

Homogeneously frozen cloud droplets are now advected in 1-D in the same manner as cloud water, CN and vapour, to improve the dynamical coupling with the vapour field. Homogeneously frozen droplets are grown as cylindrical particles, with an evolving bulk density and shape predicted by the particle-growth scheme. Homogeneous aerosol freezing as predicted by Koop *et al.* (2000) is now included. Whenever the supersaturation with respect to ice exceeds the temperature- and size-dependent critical value corresponding to a given aerosol size-bin, all the aerosols in that size-bin are instantaneously frozen. This is an approximation to reality, since it takes a finite time for real drops to freeze. It is assumed that aerosols will always freeze homogeneously before they can activate as liquid droplets, at all temperatures colder than about $-40\,^\circ$C (see Fig. 3 of Koop *et al.* 2000; Knollenberg *et al.* 1993). Consequently, secondary droplet nucleation is only applied at temperatures warmer than about $-40\,^\circ$C.

Collision efficiencies for the freezing of supercooled raindrops in collisions with ice crystals have been incorporated, utilizing laboratory data from Lew and Pruppacher (1983) for ice columns and from Lew *et al.* (1985) for planar crystals. The observed dependence of these collision efficiencies on ice-particle size, bulk density and axial ratio are included (by converting the published plots to multi-dimensional look-up tables). For the smaller supercooled raindrops (<0.2 and <0.6 mm for collisions with

columnar and planar particles, respectively) no empirical data are available: their drop–ice collision efficiency is approximated by the drop–drop value for a hypothetical drop of the same mass as the colliding ice particle, as in the HUCM. Finally, accretion of supercooled rain or drizzle by very large ice particles has been included. The collision efficiency for the collection of supercooled rain and droplets by larger ice particles is now dependent on the bulk density of the ice and on the masses of each colliding pair of particles, with HUCM data for the riming of graupel and hail being applied. The density of ice from accreted rain is that of pure ice.

As with previous versions of the EMM, the terminal velocity of ice is determined by relations between its Reynolds and Best numbers, and between its Best number, particle mass and size, as presented by Pruppacher and Klett (1997) for cylindrical and spheroidal shapes of particle, respectively. For graupel, a comprehensive set of relations between the Best and Reynolds numbers from Rasmussen and Heymsfield (1987) is applied.

The time step for the prescribed evolution of cloud dynamics, and for the solution of the stochastic collection equation for coagulation and collisional nucleation processes, is 2 s. The tracing of trajectories, evaluation of riming and vapour growth of particles, and solution of empirical equations for particle shape/density, are all performed on a time step of 0.1 s.

3. OBSERVED STORM CONDITIONS AND MODEL CONSTRAINTS

(a) *Case synopsis and model meteorological inputs*

The case simulated by the EMM control simulation is that of 18 July 2002 from the CRYSTAL-FACE campaign. The campaign included Twin Otter and Citation aircraft, which both flew over the peninsula on this day. The Twin Otter flew mostly in the boundary layer in the storm's environment and carried a suite of aerosol instrumentation including a Differential Mobility Analyser (DMA). The Citation spent more time at mid-levels and performed traverses of the updraughts and anvil cirrus of storm cores. The Citation was equipped with standard meteorological instrumentation and cloud microphysical sensors including a Forward Scattering Spectrometer Probe (FSSP), a Particle Measuring System two-dimensional cloud and precipitation probe, or 2-DC probe, for counting hydrometeors, the King probe for measuring liquid cloud-water, the Counterflow Virtual Impactor and the Continuous Flow Diffusion Chamber (CFDC) for measuring aerosol activation. Finally, the NASA WB-57 aircraft, also carrying several aerosol and cloud probes, observed anvil outflows and the upper-tropospheric environment during CRYSTAL-FACE.

Strong Cb storms were popping up over the southern tip and south-east coastal region of the Florida peninsula on the afternoon of 18 July, in an environment of weak low-level winds and strong upper-level north-easterly shear. The temperature and humidity structure of the environment was observed by sondes released from ground sites on the peninsula. The convective available potential energy over the South Florida region was over 2000 J kg^{-1}, among the highest values observed during the experiment, while the highest cloud tops reached about 15 km which was slightly above average (Sherwood *et al.* 2004). The cloud base sampled by the aircraft was at 0.8 km AMSL (22 °C), and the freezing level was at 5.9 km AMSL. The boundary-layer aerosol content observed by the Twin Otter was more nearly continental than maritime. A CCN/aerosol closure study for CRYSTAL-FACE shows that if ammonium sulphate is assumed to be the aerosol chemical composition then there is an accurate treatment of CCN activation on this day (VanReken *et al.* 2003).

As described previously, the EMM requires several meteorological inputs, including the cloud-base and cloud-top altitudes given above. A top height of 14 km was used, since this was a more typical value, although some clouds reached higher levels. Updraught velocity was prescribed based on the penetration by the Citation after 1932 UTC, where a peak updraught speed of almost 24 m s^{-1} was measured at about 11 km AMSL ($-34\,^\circ$C) in the mixed-phase region. The turbulent dissipation rate from the Citation data had a mean value of about 700 cm^{2}s^{-3} at about 11 km AMSL. The peak updraught speed in the model was set at 25 m s^{-1} at 11 km AMSL and 3 m s^{-1} at cloud base. The vertical wind shear between 1 and 11 km AMSL was obtained from sonde data, and was about 1.5 m s^{-1}km^{-1}, which was the input for the model.

A size-resolved vertical profile of aerosol-number mixing ratio ($N_{\text{env},j}(z)$) for the model was generated by combining the profiles of size distribution from the WB-57 and Twin Otter aircraft in the upper and lower troposphere, respectively. The gap between the two ranges of altitude from these aircraft was filled with an interpolation that matched the total aerosol concentration in all size-bins to that observed with the FSSP probe on the Citation aircraft at each level. The Twin Otter particle-size distribution was observed with the DMA (<950 nm) and Passive Cavity aerosol Spectrometer Probe (0.1–3 microns), being normalized by the total number concentration of aerosols from the Condensation Particle Counter. The aerosol size distribution from the WB-57 was measured in the nucleation mode with the Nucleation-Mode Aerosol Size Spectrometer (data from 19 July were used because there was no WB-57 flight on 18 July).

The CFDC instrument on the Citation measured an environmental IN concentration that was up to about 1.5 times the value obtained from the Meyers *et al.* (1992) formula for condensation-deposition freezing. Consequently, in the model the environmental concentration of IN activated at each level was determined by multiplying the temperature-dependent value from Meyers *et al.* by this observed factor. The formula by Meyers *et al.* was arbitrarily extrapolated to $-30\,^\circ$C for the lowest temperature of IN activation; a sensitivity test (see subsection 4(f)) did not reveal any appreciable sensitivity to the choice of its value.

(b)   *Determination of model physical parameters*

Aircraft observations of convective updraughts on 18 July during CRYSTAL-FACE were analysed to estimate the contribution to the horizontally averaged (indicated by $\langle\,\rangle$) rate of coagulation from the correlation between spatial 3-D deviations, $\langle N'(m)N'(q)\rangle$, of the particle concentration (see the third and fourth correlation terms of Eq. (2) in Stevens *et al.* (1998)) at spatial scales >0.1 km. Here, N is the particle concentration while m and q are masses of colliding particles. This correlation was observed to be at least an order of magnitude less than the product of the updraught-average concentrations, $\langle N(m)\rangle\langle N(q)\rangle$. A 'large-scale eddy-enhancement factor' may be defined here as the average over values of m and q at a given level of:

$$\Theta = 1 + \langle N'(m)N'(q)\rangle/(\langle N(m)\rangle\langle N(q)\rangle).$$

This eddy-enhancement factor is applied to the collision kernels for coagulation processes in the 1-D model, in order to account for the 3-D inhomogeneity of the particle concentration in the real cloud on spatial scales >0.1 km. It has observed values in the range of about 1.01 to 1.1 for Citation traverses of Cb updraughts at levels in the mixed-phase region on 18 July 2002 (a value of 1.1 is applied in the model). Its proximity to unity suggests that, for the particular cloud being simulated, collision-coalescence may be adequately predicted in a 1-D framework if the average cloud-water properties are accurate.

A value of 2.7 for the entrainment parameter, E, was selected so as to match, at all levels in the updraught, the mixing ratio of a passive tracer in the EMM with that predicted in the 3-D cloud model of Fridlind *et al.* (2004). Aircraft observations analysed by Fridlind *et al.* indicate that the secondary droplet nucleation aloft occurs primarily at the edges of the updraught in regions of entrainment for Cb cells on this particular day of CRYSTAL-FACE. In such regions, the supersaturation is expected to be substantially lower than the average value for the entire width of the updraught, because values of the vertical air velocity are low and also due to dilution with dry environmental air. Hence, an 'effective supersaturation' for predicting secondary droplet nucleation was assumed to be a prescribed fraction, 0.1, of the local value of the predicted average supersaturation at a given level, at altitudes above where the average fraction of cloud-base air is 50% (4 km AMSL). This fraction was selected so as to match the predicted droplet concentration with that observed. For inputs to the droplet nucleation scheme, ammonium sulphate was assumed for the chemical composition of the aerosol (see subsection 3(a)).

(c)   *Comparison of available aircraft observations with control*

The simulations were run for 75 minutes, during which time the model cloud top was lifted by a sequence of thermals from 5 km AMSL to the maximum cloud-top altitude of 14 km AMSL. The predicted vertical profiles of certain microphysical properties of the storm updraught have been averaged over the entire glaciated period of the simulation at each level, and are compared here with observed profiles (see subsection 3(b)). Figures 1 and 2 demonstrate that cloud-water properties were adequately predicted, given the spread of the observed values. (Here, as elsewhere in the present paper, 'concentration' refers to the number of particles per unit volume of air, not the mass of particles.) All the activated droplets disappear either by homogeneous freezing or by evaporation near the $-36\,°C$ level. As was found by Heymsfield and Sabin (1989), the homogeneous freezing of droplets occurs over a very narrow temperature range of about 1 degC. The predicted and observed profiles of cloud-droplet concentration tend to decrease with height throughout the entire depth of the cloud, largely due to intensification of accretional losses from riming and accretion onto rain during ascent. Secondary droplet nucleation makes an increasing contribution to the droplet concentration during ascent (see subsection 4(b)). Figure 3 shows observed and modelled total condensed-water content, and Fig. 4 shows particle concentrations from the model and filtered 2-DC aircraft observations.

In all cases, the simulated quantity is within one standard deviation of the observed mean value and is well within the observed range of raw data values. Given our inexact knowledge of the age of the cumulus turrets sampled by the Citation, and the sparseness and imperfect collocation of various observations, we believe the agreement is adequate.

The predicted liquid fraction (the fraction by mass of the total mixing ratio of cloud-water, rain and ice, that is liquid) in the updraught decreases monotonically with height from 100% at the freezing level to about 10% at 11 km AMSL just below the anvil base. It approaches zero rapidly just above 11 km AMSL, above which all remaining liquid freezes. This is consistent with aircraft observations aloft. Only about 10–15% of all particles >0.1 mm are observed to be spherical in our inspection of the 2-DC aircraft observations, for the traverse at $-35\,°C$ (11.3 km AMSL in the model) by the Citation at 1933 UTC. Similarly, the model predicts that only about 10% of particles >0.1 mm are (round) liquid raindrops at this level, while the remaining 90% of particles >0.1 mm are predicted to be ice particles that are not round, such as frozen drops (axial ratio, AR, predicted to be 0.6) and H-M splinters (AR predicted to be 0.4). The lack of sphericity
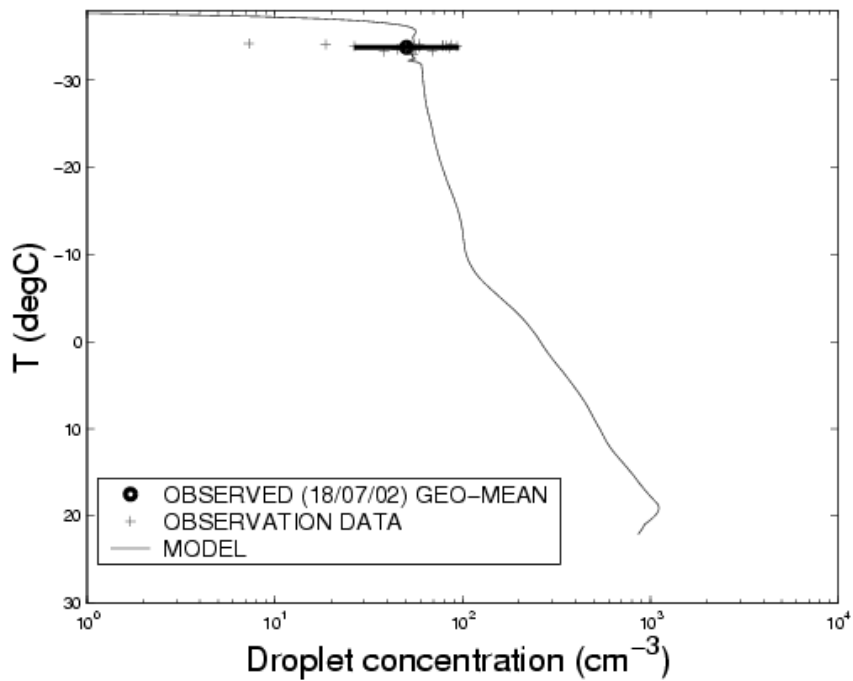
Figure 1. Mean droplet concentrations in a deep cumulus updraught observed by the Forward Scattering Spectrometer Probe and those predicted by the Explicit Microphysics Model. The horizontal bar centred on the observed mean ('o') is two standard deviations wide.
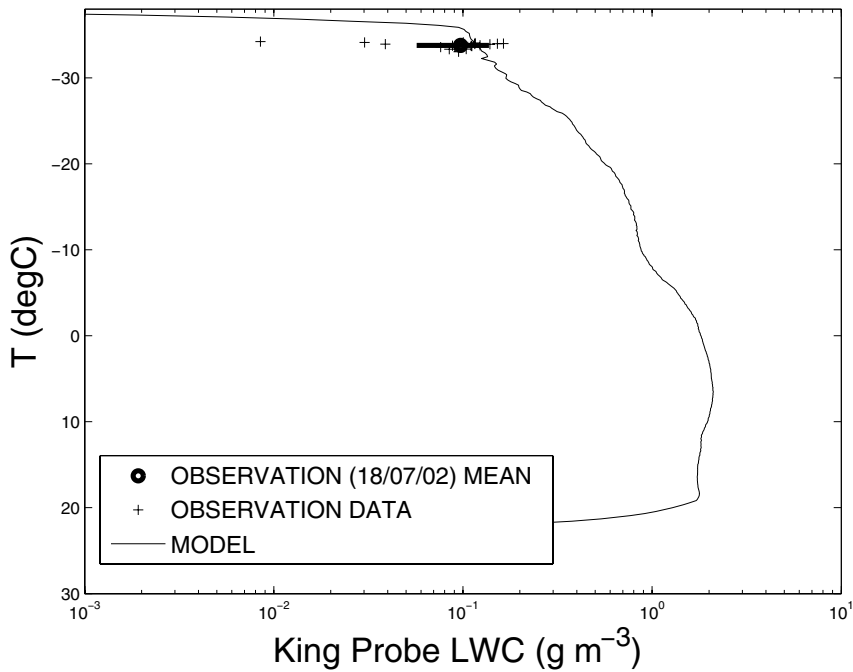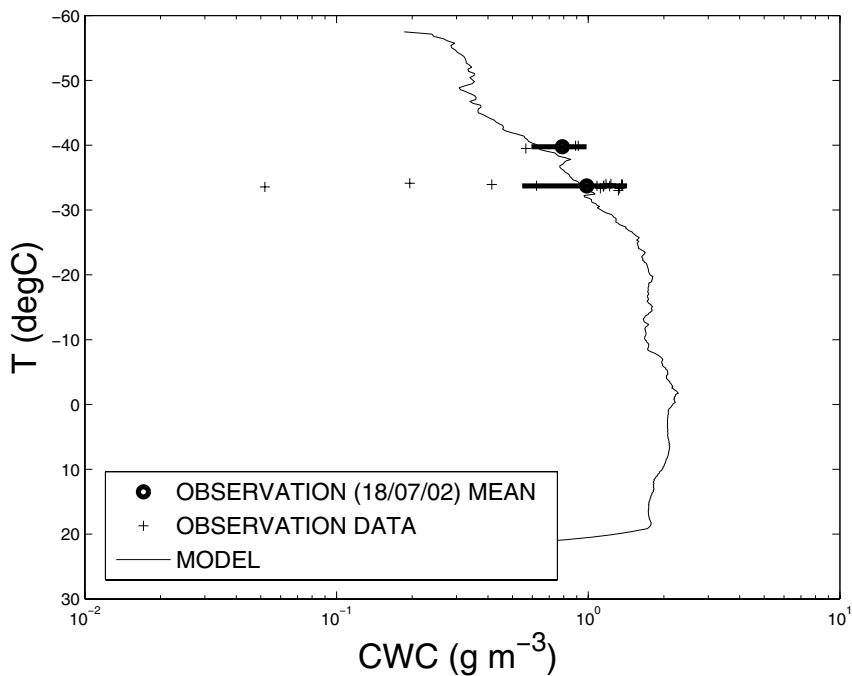

Figure 2. Mean liquid water content (LWC) in a deep cumulus updraught observed with the King probe and those predicted by the Explicit Microphysics Model. The horizontal bar centred on the observed mean ('o') is two standard deviations wide.

Figure 3. The measured condensed-water content observed in a deep cumulus updraught for all hydrometeors (arithmetic and geometric means are given) and that predicted by the Explicit Microphysics Model. The horizontal bars centred on the observed means ('o') are two standard deviations wide.
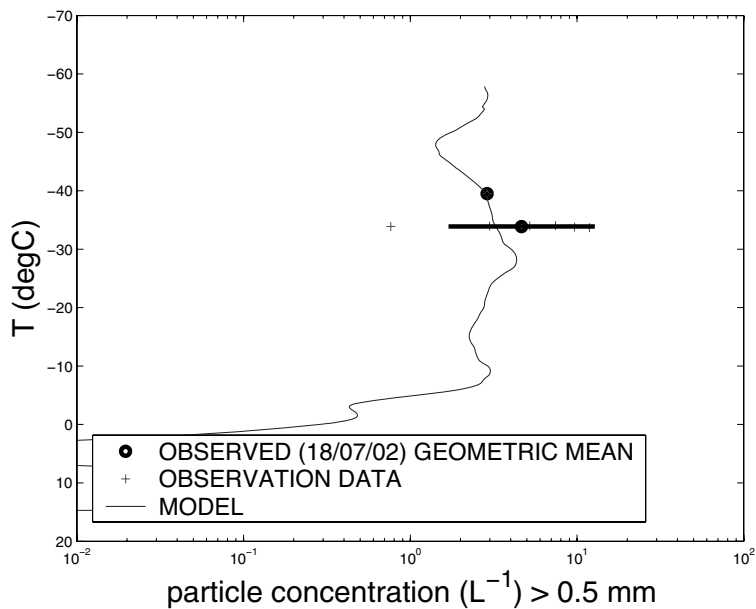
Figure 4. Filtered (>0.5mm) 2-DC (see text) particle concentrations observed in a deep cumulus updraught, and those predicted by the Explicit Microphysics Model. The increase with height towards the anvil top in the model is an artifact of the time-averaging, reflecting the fact that the ascent of thermals (with high ice concentrations) slows towards cloud top.
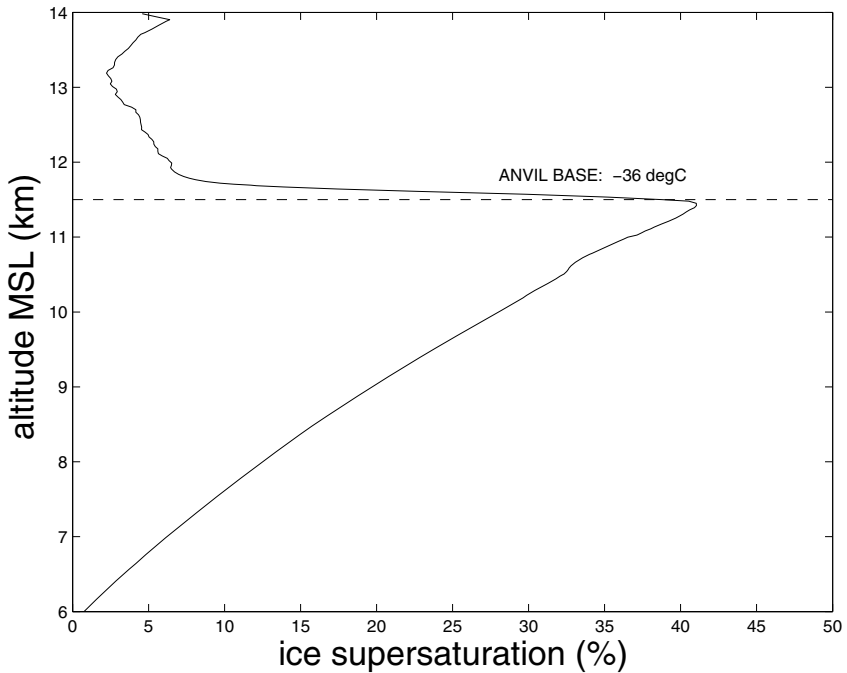
Figure 5. Vertical profile of supersaturation with respect to ice in a deep cumulus updraught in the Explicit Microphysics Model.

of frozen drops at this altitude in the control simulation is due to their vapour growth, as they are too small (0.1–0.2 mm) to rime efficiently. This validates the particle-growth scheme in the EMM.

Finally, although the ice concentration is fairly uniform with height (about 20–40 L^{-1}), the average ice-water content reduces with height from 0.9 to 0.1 g m^{-3} over the entire depth of the anvil. This is at least qualitatively consistent with aircraft observations of a decrease of ice-water content with decreasing temperature in tropical convective anvil cirrus in the vicinity of Kwajelein in the west Pacific (Brown and Heymsfield 2001). In the model nearly all ice mass below the anvil resides in graupel, and ice particles are far less numerous than liquid droplets, despite contributing comparably to condensed mass at most levels. Figure 5 illustrates the vertical profile of supersaturation with respect to ice. Above the anvil base, the ice supersaturation is <10% mostly, which is well below the threshold for homogeneous aerosol freezing. Figure 6 displays the particle size distribution from the updraught at −50 °C (about 13 km AMSL). Most anvil ice particles are in the size range 10–50 microns.

4.   RESULTS: SENSITIVITY TO NUCLEATION PROCESSES

Results are presented here from a sequence of sensitivity studies dealing with the key nucleation processes, in order to assess the impact of various nucleation processes on the anvil.

The mixed-phase region extends from the freezing level at 5.9 km AMSL to the anvil base at about 11.5 km AMSL (−36 °C). Cloud droplets that reach the anvil base will freeze homogeneously there, or else simply evaporate. The anvil extends from about
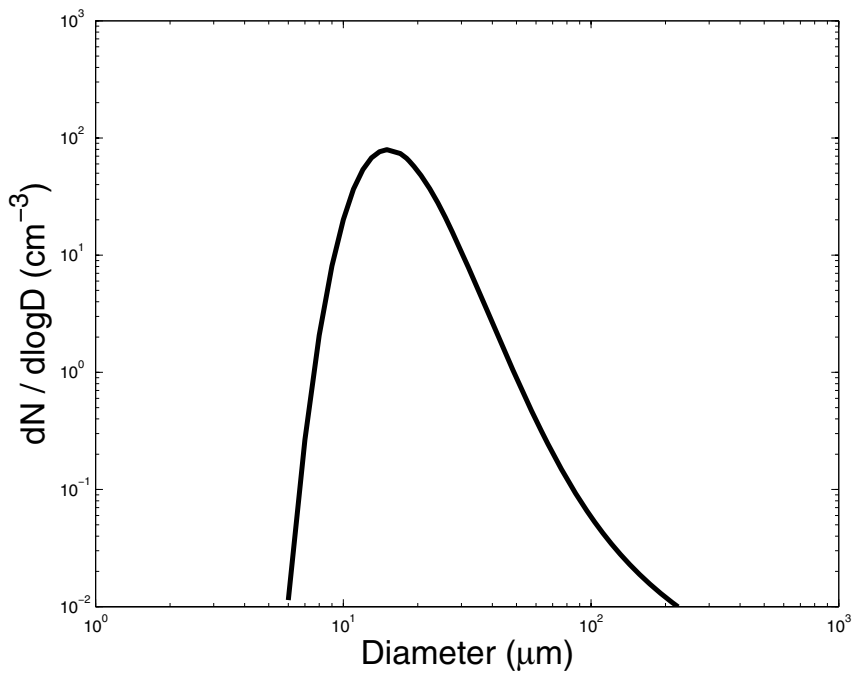
Figure 6.   The particle size distribution in a deep cumulus updraught given by the Explicit Microphysics Model for ice particles at the $-50\,^\circ$C level. Here, dN is the ice concentration (cm^{-3}) in d$(\log D)$, where D is the particle diameter.

11.5 km AMSL to the assumed maximum cloud-top level of 14 km AMSL. The H-M region is located at 6.5 to 7.4 km AMSL (-3 to $-8\,^\circ$C). This is where the H-M process of ice multiplication is active. Unless otherwise stated, results are taken from the updraught of the storm.

(a)   *No homogeneous freezing*

A model run was performed with homogeneous freezing of droplets, rain and aerosols prohibited (the case with no homogeneous freezing), so that droplets could remain as supercooled water to arbitrarily low temperatures unless frozen via activation of IN. This run was compared with the control.

Figure 7 shows that the total ice concentration at all levels in the anvil was about three orders of magnitude lower in the no-homogeneous-freezing case than in the control. The discontinuity in total ice concentration caused by the homogeneous freezing of droplets at the anvil base in the control was completely eliminated; however, the ice concentration in the mixed-phase region of the updraught remained almost unaltered. The ice mixing ratio was reduced by about 1 g kg^{-1} at most levels in the anvil in the no-homogeneous-freezing case relative to the control. The mixing ratio of supercooled cloud water was increased from zero to values of about 0.5 g kg^{-1} in the anvil when homogeneous freezing was excluded. The peak in ice crystal concentration near 7 km AMSL is due to the H-M process being active in both simulations.

Anvil crystals are about an order of magnitude larger in the case with no homogeneous freezing relative to the control. Figure 8 demonstrates that they are about 200–300 kg m^{-3} less dense. They are also slightly less columnar, with an *AR* that is closer to
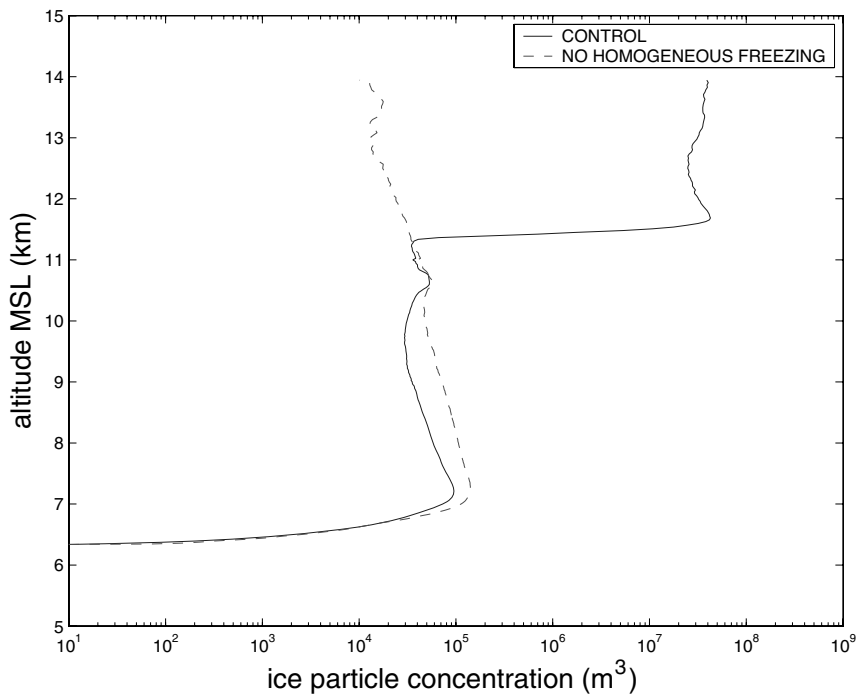
Figure 7.   Comparison of the vertical profile of total ice concentration in a deep cumulus updraught predicted by the Explicit Microphysics Model with no homogenous freezing, with that from the control run.
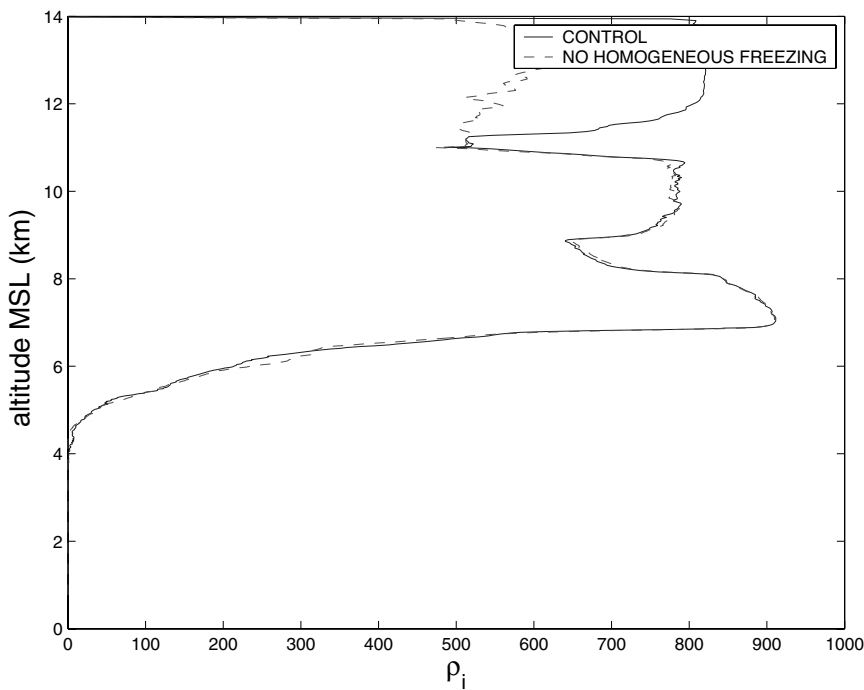

Figure 8.   As Fig. 7 but for the bulk density of ice, ρ_i.

unity (lower by about 0.5). These changes arise because anvil crystals are formed by primary nucleation (i.e. condensation-freezing when IN activate) in the no-homogeneous-freezing case, and are larger (by about 0.2 mm) having experienced much vapour growth at water-saturated conditions in the mixed-phase region before entering the anvil.

In summary: about 99.9% of all anvil ice particles (representing about half of the total ice mass in the anvil) are nucleated by homogeneous freezing in the updraught of this particular model cloud, in the control simulation. This mostly involves the freezing of supercooled cloud-droplets at the anvil base. Consequently, all other nucleation processes can only significantly affect the anvil ice concentration insofar as they alter the amount of supercooled condensate available for homogeneous freezing in this model cloud.

(b) No in-cloud CCN activation

The next run was performed with both secondary droplet nucleation and homogeneous aerosol freezing prohibited (the primary-only case). Secondary droplet nucleation involves the activation of CCN as cloud droplets anywhere in the 'interior' of the cloud (i.e. at least 500 m above the cloud base), while homogeneous aerosol freezing refers to freezing of haze particles that survive the entire updraught without activating. This simulation therefore distinguishes the role of primary droplet nucleation (activation of droplets near the cloud base), traditionally viewed as the main source of droplets.

Figures 9 and 10 demonstrate the impact that secondary droplet nucleation has on the concentration of anvil ice crystals and supercooled droplets in the storm, by comparing the model run having only primary nucleation with the control run. Most of the droplets in the upper half of the mixed-phase region are clearly generated by secondary droplet nucleation in the control. The droplet concentration is reduced by about two orders of magnitude near the anvil base in the primary-only case relative to the control.

Secondary droplet nucleation is only significant at levels more than about 3 km above the cloud base, because the vertical velocity is lower and the droplet concentration higher at levels nearer the cloud base. In the upper half of the mixed-phase region, the rain mixing ratio in the primary-only case is reduced by <0.05 g kg^{-1}, since the warm-rain process is less active in the absence of copious cloud-water aloft. This result is consistent with the findings of Pinsky and Khain (2002) that secondary droplet nucleation accelerates coalescence. The cloud-water mixing ratio is also reduced by about 0.5–1 g kg^{-1} at those levels.

In the anvil, the ice concentration is reduced by about two orders of magnitude at most levels. The mean diameter of anvil crystals is increased by one order of magnitude (from about 0.04 to about 0.4 mm) at most levels above 11 km AMSL in the primary-only case relative to the control, due to fewer crystals competing for the available vapour. Crystals are predicted to be less columnar and less dense in the anvil of the primary-only case: their *AR* is about 0.5 lower and their bulk density is about 200–300 kg m^{-3} lower, relative to the control. The bulk density is lower because the particles grow as bullets to larger sizes in the primary-only case near the anvil base, and the bulk density of bullets decreases during growth. This extra bullet growth is due to the much larger supersaturations reached aloft.

In summary: secondary droplet nucleation followed by homogeneous droplet freezing is the source of ice particles in the anvil updraught of the control simulation. This is partly because most primary droplets—nucleated near cloud base (0.8 km AMSL) in the updraught—never reach the anvil base (11.3 km AMSL), being depleted by accretion onto precipitation or detrainment in the underlying mixed-phase region. This depletion
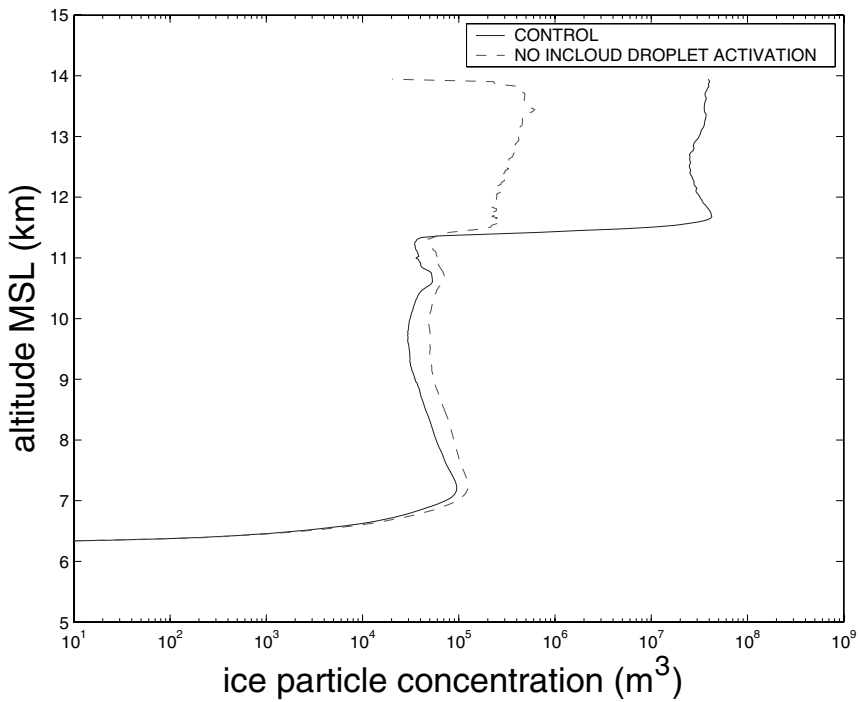
Figure 9. Comparison of the vertical profile of ice particle concentration in a deep cumulus updraught predicted by the Explicit Microphysics Model with no in-cloud droplet activation, with that from the control run.
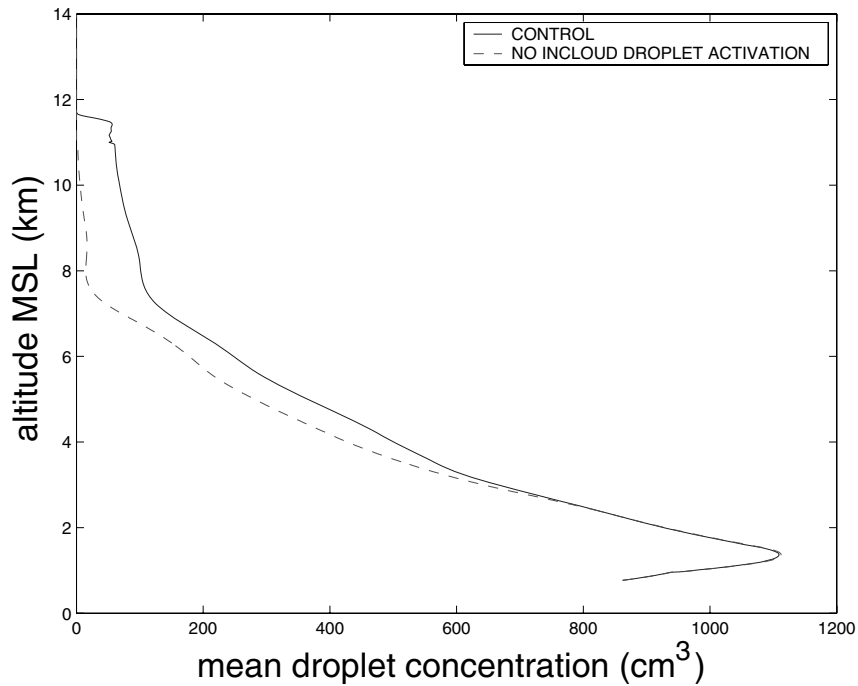

Figure 10. As Fig. 9 but for the mean predicted droplet concentration.

of primary droplets contributes to an increase of the average supersaturation with height, especially above the freezing level, which causes in-cloud activation of CCN aloft. The shape and bulk density of anvil crystals, which are explicitly predicted by the model, are appreciably sensitive to the nature of droplet nucleation in the updraught.

(*c*)   *No warm-rain process*

A model run was performed with all coalescence prohibited (the no-coalescence case). This run was compared with the control.

Microphysical properties in, and below, the anvil were found to be radically altered by the exclusion of coalescence. The rain mixing ratio was reduced to zero throughout the updraught and at subzero levels in the SCR. The cloud-water content was increased by <3 g kg^{-1} (by up to about 200%) in the updraught above 6 km AMSL and by <0.5 g kg^{-1} (about 100%) in the SCR. In the updraught of the no-coalescence case, the average cloud-droplet diameter was found to be about 5–10 μm higher at most levels in the mixed-phase region relative to the control. This is because accretion of cloud droplets by precipitation in the control occurs preferentially at larger droplet sizes, so that coalescence tends to reduce the average droplet size in this particular model cloud.

Figures 11 and 12 depict the vertical profiles of the average number concentrations of ice particles and droplets, respectively, in the model run with all coalescence prohibited and in the control. In the anvil, the total ice concentration is at least half an order of magnitude higher in the no-coalescence case, due to more droplets being available for homogeneous freezing than in the control. The ice mixing ratio in the anvil is found to be increased by about 200% relative to the control, because there is much less precipitation and the condensed water is much less likely to fall out of the updraught. In the mixed-phase region of the updraught, the ice mixing ratio is reduced to extremely low values in the no-coalescence case; at these levels raindrop freezing dominates the ice mass budget in the control simulation. The absence of frozen rain causes the H-M process to be entirely inactive in the updraught of the no-coalescence case. H-M splinters in the control simulation account for the peak in total ice concentration at 7 km AMSL. Hence, below the anvil base the total ice concentration is reduced by at least one order of magnitude at most levels in the no-coalescence case relative to the control.

Anvil crystals are found to be less dense and less columnar in the no-coalescence case than in the control. Figures 13 and 14 show the explicitly predicted values of mean *AR* and bulk density, respectively, in the model run with all coalescence prohibited and the control. In the anvil, the average bulk density is reduced by about 100 kg m^{-3} while the *AR* is reduced from almost 2 in the control to about 1.3 in the no-coalescence case.

Both explicitly predicted profiles of *AR* display columnar ($AR > 1$) growth in columnar temperature regimes at 6.5–7.5 km AMSL and 9.5–11.5 km AMSL, and similarly for planar growth ($AR < 1$) at 7.5–9.5 km AMSL, as expected for vapour growth. The absence of frozen raindrops and H-M splinters in the no-coalescence case causes the average value of *AR* to be governed by the shape of primary crystals. The planar character of primary crystals is apparent from the low values of *AR* at 7.5–9.5 km AMSL in the no-coalescence case.

In summary: raindrop freezing is found to account for most of the ice mass in the mixed-phase region of the control updraught. In the anvil, however, homogeneously frozen cloud water is more important. The mass of cloud water reaching the anvil is very sensitive to whether the warm-rain process is present. Crystal properties are similarly sensitive.
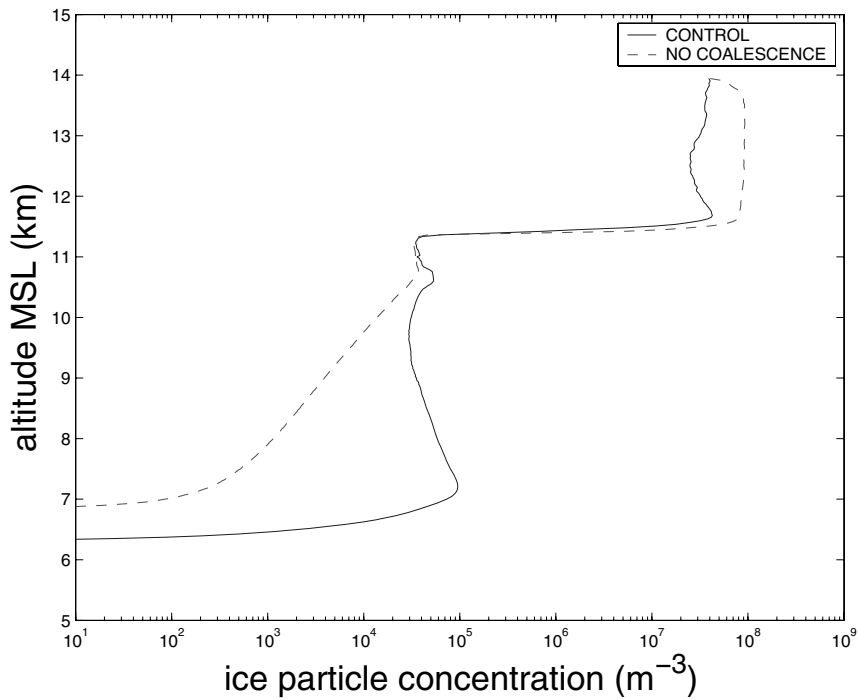
Figure 11. Comparison of the vertical profile of total ice concentration in a deep cumulus updraught predicted by the Explicit Microphysics Model having no coalescence, with that from the control run.
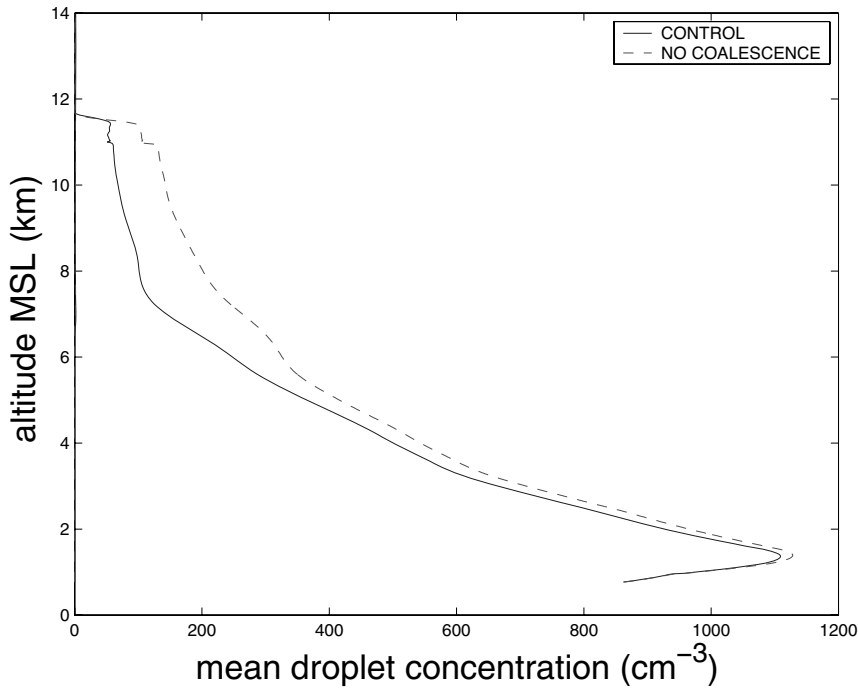
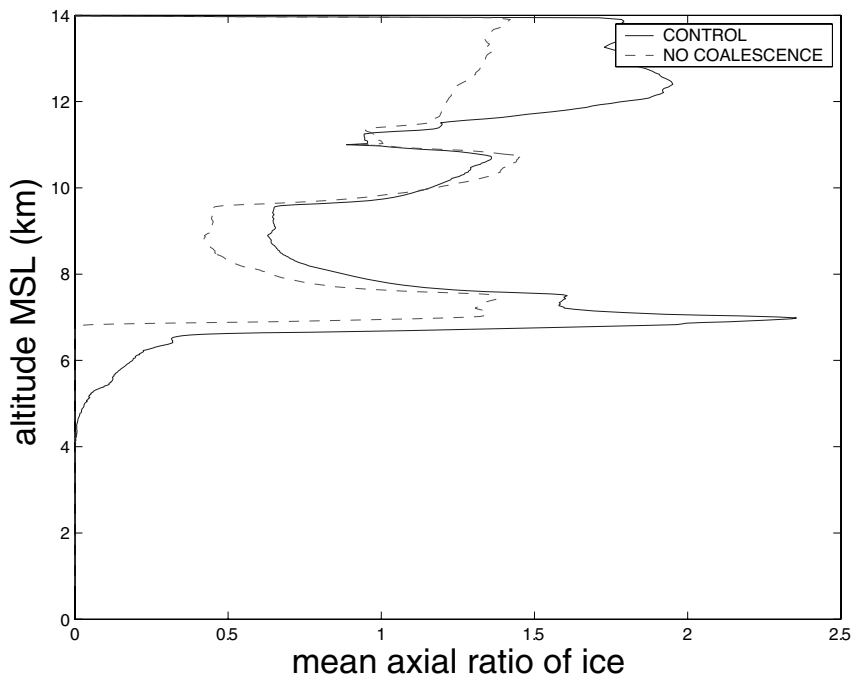Figure 12. As Fig. 11 but for the mean droplet concentration.

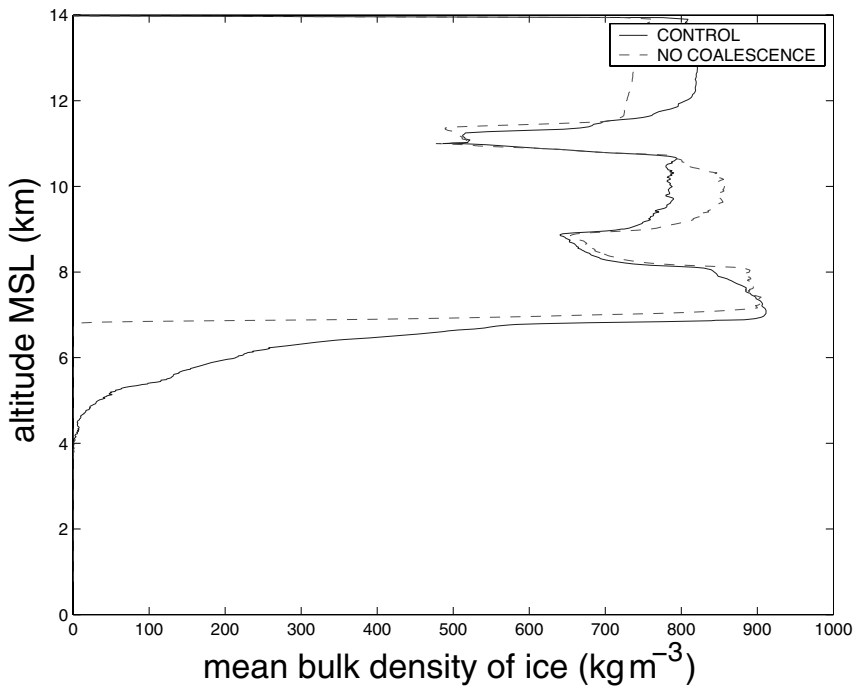Figure 13.   As Fig. 11 but for the mean axial ratio of ice.

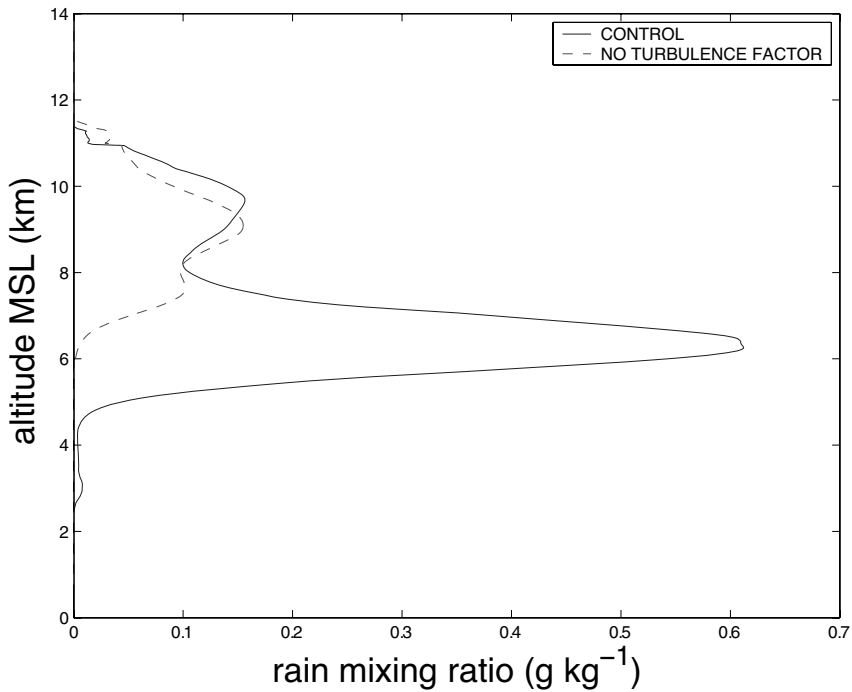Figure 14.   As Fig. 11 but for the mean bulk density of ice.

Figure 15.   Comparison of the rain mixing ratio profile in a deep cumulus updraught predicted by the Explicit Microphysics Model having no turbulence in the droplet/raindrop coalescence process, with that from the control run.

(d)   *No turbulence enhancement factors for coalescence*

A run was performed with the turbulence enhancement factors removed from the droplet/raindrop coalescence process (the zero-turbulence case). Turbulent enhancement of other accretional processes, such as riming, aggregation and collisional raindrop-freezing, was not altered.

Figure 15 shows that the lower of the two peaks of rain mixing ratio, which were found in the control, vanishes in the zero-turbulence case. No rain is found below the 6 km AMSL level in the zero-turbulence case. The onset of coalescence in updraught parcels is drastically delayed by the absence of turbulence effects. Figure 16 demonstrates that the average concentration of supercooled cloud-droplets is enhanced by up to about 50% in the interior of the mixed-phase region in the zero-turbulence case. This is due to lower rates of accretion of droplets by frozen and supercooled raindrops. However, the sensitivity of the supercooled droplet concentration appears to decrease with height towards the anvil base. The cloud-water content in the mixed-phase region is increased by about 1–2 g kg^{-1}. In the mixed-phase region, the peak in total ice concentration associated with H-M splinter generation in the control at about 7 km AMSL vanishes in the zero-turbulence case since frozen raindrops are scarcer.

Figure 17 shows that in the anvil the average ice concentration is enhanced by about 20% at most levels in the zero-turbulence case relative to the control, because of higher concentrations of supercooled droplets. Figure 18 illustrates that at most anvil levels there is a reduction in the mean ice diameter by a few microns relative to the control, due to increased competition between crystals for the available vapour. There are also slight reductions in the anvil crystal *AR* and bulk density.
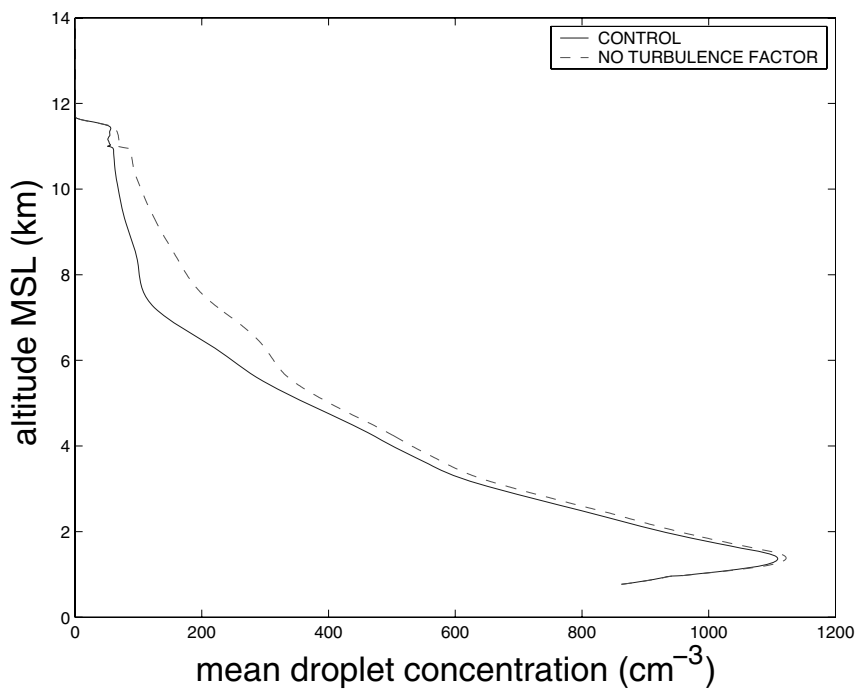
Figure 16.   As Fig. 15 but for the mean droplet concentration.
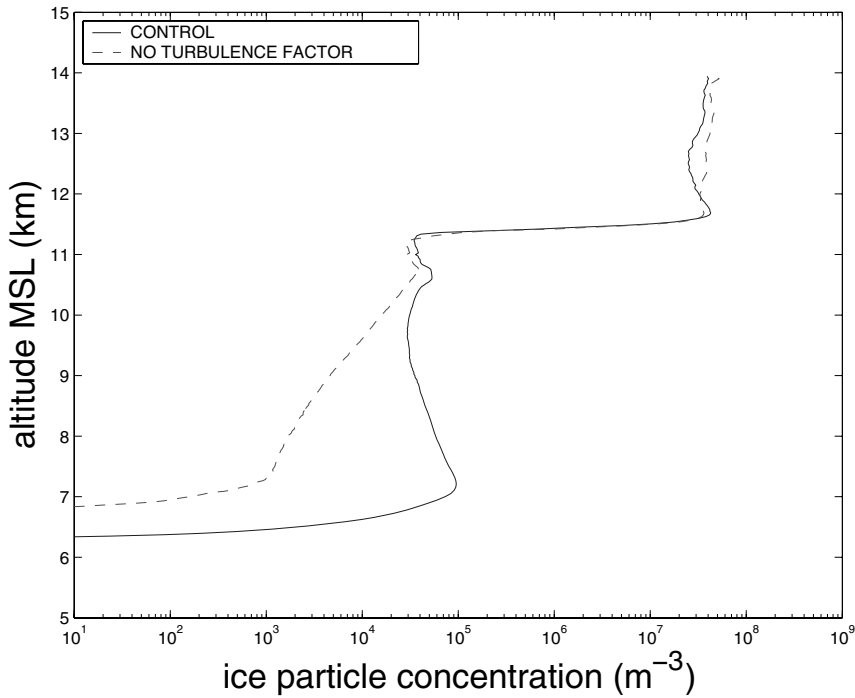

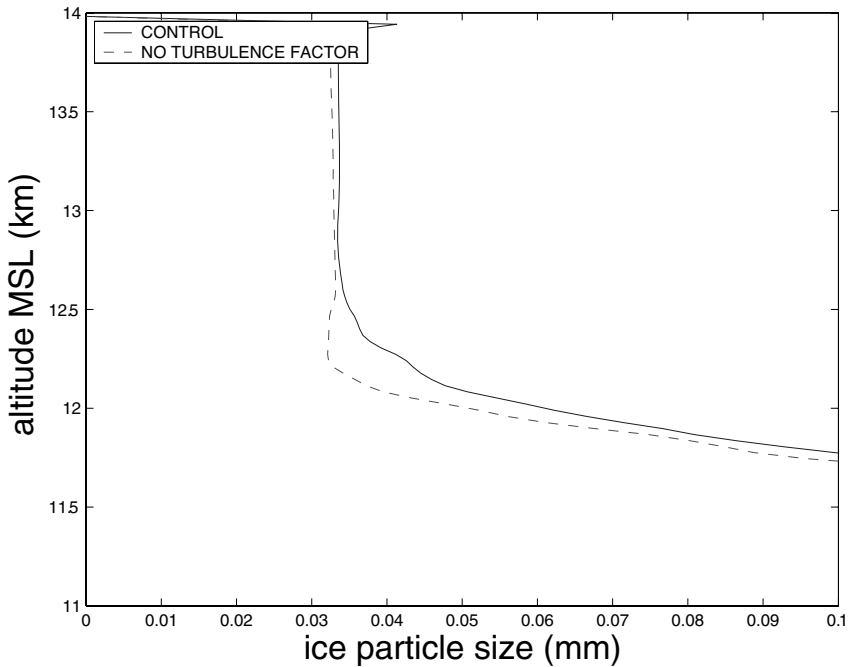Figure 17.   As Fig. 15 but for the ice particle concentration.

Figure 18.   As Fig. 15 but for the mean ice diameter in the anvil.

Additionally, two further perturbation simulations were performed in which the difference between the turbulent enhancement factor and unity for coalescence was doubled and halved, respectively (not shown). Every doubling of this difference represents, qualitatively, the effect of increasing the turbulent dissipation rate by a few hundred percent. The altitude of warm-rain production was found to decrease steadily with increasing turbulent enhancement, and also to intensify, as expected, between the zero-turbulence case, these two extra runs and the control. This was found to reduce steadily the supercooled-droplet concentration, reducing the anvil ice concentration. However, the H-M process was only altered in a major fashion by the total removal of turbulent enhancement from the control.

(e)   No raindrop freezing

A run was performed with heterogeneous and collisional raindrop freezing removed (the no-raindrop-freezing case). The freezing of cloud droplets and aerosols was the same as in the control run.

In the anvil, the ice concentration was found to be about 30% higher in the no-raindrop-freezing case relative to the control because of a similar fractional increase in the average droplet concentration in the mixed-phase region. The average ice diameter was lower by about 15%, while anvil crystals were less columnar (*AR* lower by about 0.5) and less dense by about 50 kg m^{-3}. The changes in crystal properties are qualitatively similar to those found when the warm-rain process was excluded (see subsection 4(c)). In the mixed-phase region, the number concentration of graupel particles is reduced by about two orders of magnitude, reflecting the fact that in the control run raindrop freezing, rather than the riming of primary crystals, is the main source of graupel.
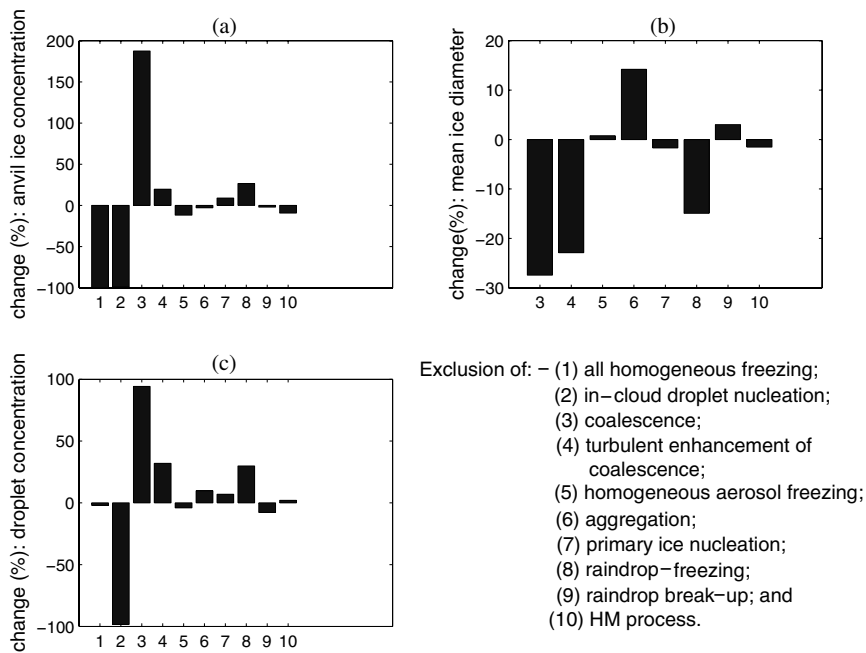
Figure 19. Percentage changes in the interior of the cloudy updraught for the ten nucleation processes studied here (see key): (a) of ice concentration in the anvil updraught, (b) of the mean diameter of ice particles in the anvil updraught; and (c) of supercooled droplet concentration changes in the 1 km layer below the anvil. The fractional changes in mean ice diameter for homogeneous freezing and in-cloud-droplet nucleation (not plotted) are about 600% and 900% respectively. HM refers to the Hallett and Mossop (1974) process of ice multiplication. See text for further details.

In summary: the higher cross-sectional area of frozen raindrops in the control run more effectively depletes droplets than in the no-raindrop-freezing case (see Johnson 1987). This means that the droplet concentration is higher in the raindrop-freezing case, with concomitant changes in the concentration and properties of anvil crystals.

(*f*) *Intercomparison of all nucleation processes*

The histograms in Fig. 19 show the average percentage changes in concentration and mean diameter of anvil ice particles, and in supercooled-droplet concentration below the anvil base, when ten particular processes (given in the key) are individually excluded from the model relative to the control simulation. Naturally, the greatest direct impact on the anvil ice concentration is from homogeneous freezing (test 1). Indirect modifications of the anvil glaciation are caused by processes associated with the nucleation of new ice particles in the mixed-phase region, such as collisional and heterogeneous raindrop-freezing (test 8) and primary nucleation of crystals (test 7). When such non-homogeneous nucleation processes are excluded, there is usually an increase in the concentration of droplets reaching the anvil base. This is because frozen precipitation particles are much more effective at accreting cloud water than are liquid particles of the same mass (see Johnson 1987). However, by far the greatest indirect impact on the anvil glaciation is from the warm-rain process (test 3). The warm-rain process exerts a massive impact on the anvil ice concentration, because it accounts for most of the mass of both liquid and frozen precipitation generated in the control simulation. Hence, the warm-rain process causes the depletion of most of the cloud

water in the mixed-phase region. For this reason, turbulent enhancement of coalescence produces a modification of the anvil glaciation that is comparable to, or exceeds, the indirect impacts from (non-homogeneous) ice nucleation processes in the mixed-phase region.

In-cloud droplet nucleation (test 2) produces a major impact on the anvil ice concentration. It is the source of about 99% of the number of supercooled droplets reaching the anvil base in the control simulation. Since homogeneous freezing of such droplets accounts for about 99.9% of the anvil crystals (see test 1), most of the anvil ice crystals in the control simulation must be caused by secondary droplet nucleation (see subsection 4(b)). When environmental aerosols above 5 km AMSL are neglected in a further sensitivity test with the EMM, the average concentration of supercooled droplets just below the anvil base in the updraught is reduced by about two-thirds, relative to the control.

Processes making minor contributions to the anvil ice concentration include aggregation, the H-M process, raindrop break-up and homogeneous aerosol freezing. Aggregation appears to require much longer time-scales for the production of precipitation in a deep convective cumulus cloud compared to coalescence. Homogeneous freezing of aerosols is not very significant when compared with that of cloud water, because secondary droplet nucleation usually maintains a sufficiently high concentration of droplets and anvil ice particles for the saturation ratio almost never to reach the threshold for homogeneous aerosol freezing. Some of these four nucleation processes, of limited significance for the anvil, cause appreciable modifications of the cloud-water field in the interior of the mixed-phase region. Finally, no appreciable sensitivity was found when the temperature cut-off for heterogeneous droplet freezing was changed from -30 to $-60\,^{\circ}$C.

Three extra sensitivity tests revealed that the anvil ice concentration was reduced by about 5–10% by the following exclusions: the explicit prediction of the graupel density (replaced by a constant value of $400\,\text{kg m}^{-3}$); the surface temperature of ice (fixed to the ambient air temperature); and the graupel drag coefficient (replaced by a formula from Beard (1980)). Significant perturbations of the total ice mixing ratio $> 10\%$ and of the droplet concentration were found in these extra runs. Clearly, explicit prediction of crystal properties with a particle-growth scheme is important for accuracy.

(g) *Intercomparison of turbulence effects*

Two simulations were performed with turbulent enhancement of raindrop-freezing and riming, respectively, prohibited. The anvil ice crystal concentration was quite similar to the control value, being altered by $<10\%$. This alteration is a reduction because, although the supercooled-droplet concentration is increased by the order of 1–10% in the 1 km layer just below the anvil base, homogeneous aerosol freezing appears to be less prolific in these perturbation simulations than in the control. For prohibition of turbulent enhancement of the warm-rain process, corresponding alterations of the concentration of such supercooled droplets and anvil ice particles are $+30\%$ and $+20\%$ respectively. Clearly, the turbulent enhancement of the warm-rain process produces the dominant impact on the anvil glaciation out of all the various coagulation mechanisms.

Curiously, the mixed-phase region is very sensitive to the turbulent enhancement of riming. The H-M splinter concentration is reduced by an order of magnitude when the turbulent enhancement of riming is excluded. This coincides with a similar sensitivity of the mixing ratio of large graupel particles formed by raindrop freezing in the H-M region. It appears that turbulent enhancement of riming promotes the generation of the largest, millimetre-sized graupel particles that are able to fall against the updraught's

ascent into the H-M region. However, the anvil glaciation is not very sensitive to the activity of the H-M process, because most of the anvil ice particles originate from homogeneous freezing.

5. DISCUSSION AND CONCLUSIONS

We find that the vast majority of ice particles in the simulated Cb anvil originate as homogeneously frozen cloud droplets. The hypothesis proposed by Rosenfeld and Woodley (2000) of massive homogeneous droplet freezing at the anvil base is confirmed by this result. In very broad terms, it is also consistent with the parcel model calculations by Spice *et al.* (1999). This result is not globally applicable for absolutely all Cb, since IN concentrations can sometimes be so numerous in particular dusty episodes that most of the cloud-water freezes heterogeneously, or evaporates before it can freeze homogeneously. For instance, in CRYSTAL-FACE the concentration of IN was measured to be $O(1)$ cm^{-3} during occasional Saharan dust events (DeMott *et al.* 2003), which is an increase by a factor of at least 100 beyond the control values.

Nearly all freezing droplets were created by secondary, rather than primary droplet nucleation in the model. This occurred because: (i) primary droplets from the cloud base tend to be depleted by accretion onto precipitation before reaching the anvil base; and (ii) droplet depletion aloft, in conjunction with the rapid increase with height of the vertical velocity in the updraught, combine to boost substantially the supersaturation above the freezing level. Pinsky and Khain (2002) found that the consequent nucleation of secondary droplets accelerated raindrop formation by broadening the droplet size distribution, a result duplicated here. When secondary droplet nucleation is excluded from the EMM, the amount of rain in the mixed-phase region is suppressed.

About two-thirds of the secondary droplets reaching the anvil base are formed by the activation of aerosols that have been entrained into the updraught from the lateral environment above about 5 km AMSL in the model (see also Fridlind *et al.* 2004). Consequently, very remote surface sources of atmospheric aerosol would be expected to produce an appreciable impact on anvil and cirrus glaciation. Naturally, this result depends critically on the specification of the rate of entrainment derived from the 3-D cloud model utilized by Fridlind *et al.*

Among the remaining nucleation processes, the warm-rain process produces the greatest indirect impact on the anvil ice concentration. The warm-rain process is central to the regulation of the concentration of supercooled droplets in the mixed-phase region, which determines the anvil ice concentration. This is because coalescence is the source of almost all of the mass of precipitation, whether frozen or liquid. Precipitation acts to deplete a large fraction of the cloud droplets by accretion before they can freeze homogeneously. In the mixed-phase region, the total ice mixing ratio is dominated by raindrop freezing. Without the warm-rain process, there is no H-M process in this model cloud. The explicitly predicted ice particle properties, such as axial ratio and bulk density, are also highly sensitive to the coalescence process in the mixed-phase region. The activity of the H-M process in the control, despite the peak updraught speed being >20 m s^{-1} aloft, is consistent with 3-D numerical simulations of deep convection with bulk microphysics by Aleksic *et al.* (1989; see also Ovtchinnikov *et al.* 2000).

A striking result here is that turbulent enhancement of the collision efficiency for coalescence must be accounted for if the anvil ice concentration is to be accurately predicted. Physically, this mechanism represents the modification of the relative velocities of drops of different sizes due to their inertia (see Khain and Pinsky 1995). The velocity

difference, due to turbulence, of a pair of small adjacent droplets may be comparable with their difference in terminal fall velocities. In EMM simulations presented here, it is shown that turbulent enhancement of coalescence has a greater indirect impact on the anvil glaciation than most of the (non-homogeneous) ice nucleation processes that are active in the mixed-phase region for this particular model cloud. Our simulations corroborate the result of Pinsky and Khain (2002), that the rain production rate is quite sensitive to turbulent effects. Their result is extended in this paper to cover the sensitivity of the anvil glaciation to turbulent effects. (Although giant and ultra-giant aerosol particles are not represented in the EMM here, Feingold *et al.* (1999) found that in stratocumulus clouds such giant aerosol particles tend to modify rain production appreciably only in clouds near their threshold of rain production—Cb are very far from such a threshold.)

Furthermore, it is shown that warm-rain production decreases in altitude and intensifies steadily with an increasing degree of turbulent enhancement of the warm-rain process. This steadily reduces the supercooled droplet concentration, reducing the anvil ice concentration. It can also radically alter the H-M process. It is the turbulent enhancement of the warm-rain process, rather than that of riming or raindrop freezing, that affects the anvil the most.

The present paper shows that aggregation and homogeneous aerosol freezing are not particularly important for glaciation in the updraught region of the Cb anvil in this particular model cloud, when compared with coalescence and homogeneous freezing of cloud water. Reisin *et al.* (1996) also found that aggregation is not important in deep convective clouds, partly because of low values of the sticking efficiency. The lack of homogeneous aerosol freezing in the EMM control is consistent with estimates by Knollenberg *et al.* (1993); our hydrometeor concentrations were above the low values of a few per cubic centimetre, or less than they found necessary near the anvil base for homogeneous aerosol freezing to occur in the updraught. This estimate may also be reached by scaling the analytical formula for the equilibrium supersaturation of a mono-disperse population of spherical ice particles growing only by vapour deposition. That such low values are only very rarely reached in the EMM control simulation is partly because of the activity of secondary-droplet nucleation below the anvil base, and partly due to the continental nature of the environmental CN spectrum applied here.

Generally, homogeneous aerosol freezing is obviously shut down by updraught speeds being too weak (e.g. in cirrus; see Heymsfield and Sabin (1989)) because ascent is needed to force a positive supersaturation with respect to ice. But the EMM simulations here show that homogeneous aerosol freezing can also be shut down if the updraught speed is too high, due to droplet concentrations being too high below the anvil base. Another reason why homogeneous aerosol freezing is rare in this particular model Cb updraught, is that whenever the saturation ratio exceeds the critical threshold for homogeneous aerosol freezing, the largest few aerosols freeze first to form crystals. These crystals then deplete the vapour before more aerosols can freeze, reducing the saturation ratio (see Jensen *et al.* 1998). However, in the wider context it seems plausible that once the cirrus has become detached from the convective core, the slow decline in crystal concentration could conceivably allow episodes of homogeneous aerosol freezing to occur over much longer time-scales than those simulated here.

Secondary droplet nucleation in the Cb updraught would be expected to quench some of the sensitivity of the anvil glaciation, which may explain why several processes of nucleation are found to display only a weak sensitivity here. This is because any reduction in the supercooled droplet concentration will also tend to augment the equilibrium supersaturation in updraught parcels, causing extra nucleation of secondary droplets.

Of course, the present results apply only to the particular cloud simulated in this paper, which corresponds to the moderately continental CCN concentration observed in the environment on 18 July 2002 of CRYSTAL-FACE. Updraughts with a weaker rate of increase with height of the vertical air velocity than that prescribed for this case, would force a lower supersaturation below the anvil. This would probably reduce the extent of secondary droplet nucleation. Moreover, the present analysis assumes processes of ice nucleation are known and properly quantified. In fact, there is still controversy about what the full set of mechanisms are for secondary ice formation, especially with ice break-up.

In summary: this paper demonstrates a significant sensitivity of the ice microphysics with respect to the inclusion of turbulence enhancement factors in coalescence. There is clearly a need for continued laboratory studies and theoretical research to quantify such factors. Furthermore, certain nucleation processes, such as raindrop freezing and the warm-rain process, need to be accurately represented if the anvil ice properties of deep convection are to be correctly predicted in cloud models.

REFERENCES

Aleksic, N. M., Farley, R. D. and Orville, H. D.	1989	A numerical cloud model study of the Hallett–Mossop ice multiplication process in strong convection. *Atmos. Res.*, **23,** 1–30
Beard, K. V.	1980	The effects of altitude and electrical force on the terminal velocity of hydrometeors. *J. Atmos. Sci.*, **37,** 1363–1374
Bleck, R.	1970	A fast, approximate method for integrating the stochastic coalescence equation. *J. Geophys. Res.*, **75,** 5165
Blyth, A. M. and Latham, J.	1997	A multi-thermal model of cumulus glaciation via the Hallett–Mossop process. *Q. J. R. Meteorol. Soc.*, **123,** 1185–1198
Bott, A.	1998	A numerical method for the numerical solution of the stochastic collection equation. *J. Atmos. Sci.*, **55,** 2284–2293
Brown, P. R. A. and Heymsfield, A. J.	2001	The microphysical properties of tropical convective anvil cirrus: A comparison of models and observation. *Q. J. R. Meteorol. Soc.*, **127,** 1535–1550
DeMott, P. J., Rogers, D. C. and Kreidenweiss, S. M.	1997	The susceptibility of ice formation in upper tropospheric clouds to insoluble aerosol components. *J. Geophys. Res.*, **102,** 19575–19584
DeMott, P. J., Sassen, K., Poellot, M. R., Baumgardner, D., Rogers, D. C., Brooks, S. D., Prenni, A. J. and Kreidenweiss, S. M.	2003	African dust aerosols as atmospheric ice nuclei. *Geophys. Res. Lett.*, **30,** 14, 1732, doi: 10.1029/2003GL017410
Feingold, G., Cotton, W. R., Kreidenweis, S. M. and Davis, J. T.	1999	The impact of giant cloud condensation nuclei on drizzle formation in stratocumulus: Implications for cloud radiative properties. *J. Atmos. Sci.*, **56,** 4100–4117

Fridlind, A. M., Ackerman, A. S., Jensen, E. J., Heymsfield, A. J., Poellot, M. R., Stevens, D. E., Wang, D., Miloshevich, L. M., Baumgardner, D., Lawson, R. P., Wilson, J. C., Flagan, R. C., Seinfeld, J. H., Jonsson, H. H., Vanreken, T. M., Varutbangkul, V. and Rissman, T. A.   2004   Evidence for the predominance of mid-tropospheric aerosols as subtropical anvil cloud nuclei. *Science*, **304,** 718–722

Hall, W. D.   1980   A detailed microphysical model within a two-dimensional dynamical framework: Model description and preliminary results. *J. Atmos. Sci.*, **37,** 2486–2507

Hallett, J. and Mossop, S. C.   1974   Production of secondary ice particles during the riming process. *Nature*, **249,** 26–28

Heymsfield, A. J. and Miloshevich, L. M.   1993   Homogeneous ice nucleation and supercooled liquid water in orographic wave clouds. *J. Atmos. Sci.*, **50,** 2335–2353

   1995   Relative humidity and temperature influences on cirrus formation and evolution: Observations from wave clouds and FIRE II. *J. Atmos. Sci.*, **52,** 4302–4326

Heymsfield, A. J. and Sabin, R. M.   1989   Cirrus crystal nucleation by homogeneous freezing of solution droplets. *J. Atmos. Sci.*, **46,** 2252–2264

Heymsfield, A. J., Johnson, P. N. and Dye, J. E.   1978   Observations of moist adiabatic ascent in northeast Colorado cumulus congestus clouds. *J. Atmos. Sci.*, **35,** 1689–1703

Jensen, E. J., Anderson, D. E., Selkirk, H. B., Starr, D. O. and Toon, O. B.   2004   Overview of the Cirrus Regional Study of Tropical Anvils and Cirrus Layers—Florida Area Cirrus Experiment (CRYSTAL-FACE). *Bull. Am. Meteorol. Soc.*, in press

Jensen E. C., Toon, O. B., Sachse, G. W., Anderson, B. E., Chan, K. R., Twohy, C. W., Gandrud, B., Aulenbach, S. M., Heymsfield, A., Hallett, J. and Gary, B.   1998   Ice nucleation processes in upper tropospheric wave-clouds observed during SUCCESS. *Geophys. Res. Lett.*, **25,** 1363–1366

Johnson, D. B.   1987   On the relative efficiency of coalescence and riming. *J. Atmos. Sci.*, **44,** 1671–1680

Jonas, P. R.   1996   Turbulence and cloud microphysics. *Atmos. Res.*, **40,** 283–306

Khain, A. P. and Pinsky, M. B.   1995   Drops' inertia and its contribution to turbulent coalescence in convective clouds. Part I: Drops' fall in the flow with random horizontal velocity. *J. Atmos. Sci.*, **52,** 196–206

Khain, A. P. and Sednev, I.   1996   Simulation of precipitation formation in the Eastern Mediterranean coastal zone using a spectral microphysics cloud ensemble model. *Atmos. Res.*, **43,** 77–110

Khain, A. P., Ovtchinnikov, M., Pinsky, M., Pokrovsky, A. and Krugliak, H.   2000   Notes on the state-of-the-art numerical modeling of cloud microphysics. *Atmos. Res.*, **55,** 159–224

Khain, A., Pokrovsky, A., Pinsky, M., Seifert, A. and Phillips, V. T. J.   2004   Simulation of effects of atmospheric aerosols on deep turbulent convective clouds by using a spectral microphysics mixed-phase cumulus cloud model. Part 1: Model description and possible applications. *J. Atmos. Sci.*, **61,** 2963–2982

Knollenberg, R. G., Kelly, K. and Wilson, J. C.   1993   Measurements of high number densities of ice crystals in the tops of tropical cumulonimbus. *J. Geophys. Res.*, **98,** 8639

Koop, T., Luo, B. P., Tsias, A. and Peter, Th.   2000   Water activity as the determinant for homogeneous ice nucleation in aqueous solutions. *Nature*, **406,** 611–614

Levine, J.   1959   Spherical vortex theory of bubble-like motion in cumulus clouds. *J. Meteorol.*, **14,** 653–662

Lew, J. K. and Pruppacher, H. R.   1983   A theoretical determination of the capture efficiency of small columnar ice crystals by large cloud drops. *J. Atmos. Sci.*, **40,** 139–145

Lew, J. K., Kingsmill, D. E. and Montague, D. C.   1985   A theoretical study of the collision efficiency of small planar ice crystals colliding with large supercooled water drops. *J. Atmos. Sci.*, **42,** 857–862

Meyers, M. P., DeMott, P. J. and Cotton, W. R.   1992   New primary ice-nucleation parametrizations in an explicit cloud model. *J. Appl. Meteorol.*, **31,** 708–720

Mitchell, D. 1988 Evolution of snow-size spectra in cyclonic storms. Part I: Snow growth by vapour deposition and aggregation. *J. Atmos. Sci.*, **45,** 3431–3451

Ovtchinnikov, M., Kogan, Y. L. and Blyth, A. M. 2000 An investigation of ice production in small cumuliform clouds using a 3D model with explicit microphysics. Part II: Case study of New Mexico cumulus clouds. *J. Atmos. Sci.*, **57,** 3004–3020

Phillips, V. T. J. 2001 'Simulations of the glaciation of a New Mexican storm cloud with an explicit microphysics model (EMM)'. PhD Thesis, UMIST

Phillips, V. T. J., Blyth, A. M., Brown, P. R. A., Choularton, T. W. and Latham, J. 2001 The glaciation of a cumulus cloud over New Mexico. *Q. J. R. Meteorol. Soc.*, **127,** 1513–1534

Phillips, V. T. J., Choularton, T. W., Blyth, A. M. and Latham, J. 2002 The influence of aerosol concentrations on the glaciation and precipitation of a cumulus cloud. *Q. J. R. Meteorol. Soc.*, **128,** 951–971

Phillips, V. T. J., Choularton, T. W., Illingworth, A. J., Hogan, R. J. and Field, P. R. 2003 Simulations of the glaciation of a frontal mixed-phase cloud with the Explicit Microphysics Model. *Q. J. R. Meteorol. Soc.*, **129,** 1351–1371

Pinsky, M. B. and Khain, A. 1998 Some effects of cloud turbulence on water–ice and ice–ice collisions. *Atmos. Res.*, **47–48,** 69–86
2002 Effects of in-cloud nucleation and turbulence on droplet spectrum formation in cumulus clouds. *Q. J. R. Meteorol. Soc.*, **128,** 501–533

Pinsky, M. B., Khain, A. P. and Shapiro, M. 2000 Stochastic effects of cloud droplet hydrodynamic interaction in a turbulent flow. *Atmos. Res.*, **53,** 131–169

Pruppacher, H. R. and Klett, J. D. 1997 *Microphysics of clouds and precipitation.* Kluwer Academic Publishers, Dordrecht, the Netherlands

Ramanathan, V., Pitcher, E. J., Malone, R. C. and Blackmon, M. L. 1983 The response of a spectral general circulation model to refinements in radiative processes. *J. Atmos. Sci.*, **40,** 605–630

Rasmussen, R. M. and Heymsfield, A. J. 1987 Melting and shedding of graupel and hail. I: Model physics. *J. Atmos. Sci.*, **44,** 2754–2763

Reisin, T., Levin, Z. and Tzivion, S. 1996 Rain production in convective clouds as simulated in an axisymmetric model with detailed microphysics. Part II: Effects of varying drops and ice initiation. *J. Atmos. Sci.*, **53,** 1815–1837

Rogers, R. R. and Yau, M. K. 1991 *A short course in cloud physics.* Pergamon Press, New York, USA

Rosenfeld, D. and Woodley, W. L. 2000 Deep convective clouds with sustained supercooled liquid water down to −37.5 °C. *Nature*, **405,** 440–442

Saunders, C. P. R. and Hosseini, A. S. 2000 'A laboratory study of the effect of velocity on Hallett–Mossop ice crystal multiplication'. Pp. 617–620 in Proceedings of the thirteenth international conference on clouds and precipitation, Reno, Nevada. American Meteorological Society, Boston, USA

Sherwood, S. C., Minnis, P. and McGill, M. 2004 Deep convective cloud-top heights and their thermodynamic control during CRYSTAL-FACE. *J. Geophys. Res.*, **109,** D20119, doi: 10.1029/2004JD004811

Smith, S. A. and Jonas, P. R. 1996 Observations of turbulence in cirrus clouds. *Atmos. Res.* **43,** 1–29

Spice, A., Johnson, D. W., Brown, P. R. A., Darlinson, A. G. and Saunders, C. P. R. 1999 Heterogeneous droplet freezing in orographic cirrus clouds: A numerical simulation of the microphysics. *Q. J. R. Meteorol. Soc.*, **125,** 1637–1667

Stevens, B., Cotton, W. R. and Feingold, G. 1998 A critique of one- and two-dimensional models of boundary layer clouds with a binned representation of drop microphysics. *Atmos. Res.*, **47–48,** 529–553

VanReken, T. M., Rissman, T. A., Roberts, G. C., Varutbangkul, V., Jonsson, H. H., Flagan, R. C. and Seinfeld, J. H. 2003 Toward aerosol/cloud condensation nuclei (CCN) closure during CRYSTAL-FACE. *J. Geophys. Res.*, **108**(D20)**,** 4633